IJMMM International Journal of Minerals, Metallurgy and Materials 矿物冶金与材料学报（英文版）

Gold-leaching performance and mechanism of sodium dicyanamide

Gen-zhuang Li, Jue Kou, Yi Xing, Yang Hu, Wei Han, Zi-yuan Liu, and Chun-bao Sun

Cite this article as:
Gen-zhuang Li, Jue Kou, Yi Xing, Yang Hu, Wei Han, Zi-yuan Liu, and Chun-bao Sun, Gold-leaching performance and mechanism of sodium dicyanamide, *Int. J. Miner. Metall. Mater.*, 28(2021), No. 11, pp. 1759-1768. https://doi.org/10.1007/s12613-020-2153-6

View the article online at SpringerLink or IJMMM Webpage.

International Journal of Minerals, Metallurgy and Materials
Volume 28, Number 11, November 2021, Page 1759
https://doi.org/10.1007/s12613-020-2153-6

Gold-leaching performance and mechanism of sodium dicyanamide

Gen-zhuang Li[1)], *Jue Kou*[1)], *Yi Xing*[2)], *Yang Hu*[1)], *Wei Han*[1)], *Zi-yuan Liu*[1)], *and Chun-bao Sun*[1)]

1) University of Science and Technology Beijing, School of Civil and Resource Engineering, Beijing 100083, China
2) University of Science and Technology Beijing, School of Energy and Environmental Engineering, Beijing 100083, China
(Received: 15 March 2020; revised: 22 July 2020; accepted: 23 July 2020)

Abstract: In this work, sodium dicyanamide (SD) was used as a leaching reagent for gold recovery, and the effects of the SD dosage and solution pH on the gold-leaching performance were investigated. A gold recovery of 34.8% was obtained when SD was used as the sole leaching reagent at a dosage of 15 kg/t. In the presence of a certain amount of potassium ferrocyanide (PF) in the SD solution, the gold recovery was found to increase from 34.8% to 57.08%. Using the quartz crystal microbalance with dissipation (QCM-D) technique, the leaching kinetics of SD with and without PF were studied. The QCM-D results indicate that the gold-leaching rate increased from 4.03 to 39.99 $ng \cdot cm^{-2} \cdot min^{-1}$ when the SD concentration was increased from 0 to 0.17 mol/L, and increased from 39.99 to 272.62 $ng \cdot cm^{-2} \cdot min^{-1}$ when 0.1 mol/L of PF was used in combination with SD. The pregnant solution in the leaching tests was characterized by X-ray photoelectron spectroscopy and electrospray mass spectrometry, which indicated that Au and $(N(CN)_2)^-$ in the SD solution formed a series of metal complex ions, $[AuNa_x(N(CN)_2)_{x+2}]^-$ (x = 1, 2, 3, or 4).

Keywords: gold leaching; sodium dicyanamide; QCM-D; leaching kinetics; potassium ferrocyanide

1. Introduction

Cyanide is widely used for gold leaching but can threaten the concentrator operators' safety as well as the mine environment. Significant efforts have been made to identify alternatives to cyanide for gold leaching [1–3]. In this study, we investigated the effects of the dicyanamide anion on the gold-leaching process to consider its appropriateness as an alternative cyanide-free reagent for gold leaching. Sodium dicyanamide (SD) is an important chemical intermediate that is widely used in a variety of industries in chemical additives, pharmaceuticals, coatings, and pesticides, to name a few. Sodium dicyanamide's chemical formula is $NaN(CN)_2$, within which N and CN are active centers. As such, the chemical properties of dicyanamide are relatively active.

The anionic coordination group $M(N(CN)_2)^{3-}$, which is formed by the reaction between a dicyanamide ion $(N(CN)_2)^-$ and a metal M, was first reported in 1966 [4–5]. In the 1990s, Kurmoo and Kepert [6] studied the complexes $M^{II}(N(CN)_2)_2$, in which M = Cu, Ni, Co, and Fe. The authors found that the dicyanamide ion could bridge the metal ions through its three nitrogen atoms and form an organic metal framework with a rutile-like structure. This framework is 3D-extended, based on the unit $M(—N{\equiv}C—N—C{\equiv}N—)_2$. Metal–dicyanamide complexes $M^{II}(N(CN)_2)_2$ can be formed at room temperature through the reaction of aqueous solutions of transition-metal nitrate hexahydrates with an aqueous solution of SD. Zhang *et al*. [7] has also noted that $(N(CN)_2)^-$ is versatile in the self-design of polymeric metal structures. $(N(CN)_2)^-$ always behaves as a bridge that links two or three metal centers to form 1D-, 2D-, or 3D-extended polymers with the array $M—N{\equiv}C—N—C{\equiv}N—M'$.

Kohout *et al*. [8] found $(NCO)^-$, $(C(CN)_3)^-$, and $(N(CN)_2)^-$ to be very similar species that conform to the pseudohalide concept. Therefore, $(N(CN)_2)^-$ appears as a pseudochalcogeno-cyanate and has similar chemical properties. Like the ion $(NCO)^-$, $(N(CN)_2)^-$ is capable of having coordinated reactions with some metals. For example, in the coordination sphere of Cu, Ni, Pd, and Pt, with the presence of $(N(CN)_2)^-$, a nucleophilic addition occurs to produce a new anionic chelating ligand [1].

In the $(N(CN)_2)^-$ ion, there exist two kinds of nitrogen atoms —amide and amino. Compared to amide nitrogen atoms, terminal amino nitrogen atoms have a higher charge density [8]. As such, metal is more likely to coordinate with the terminal nitrogen atoms. There are some exceptions, such as in the anionic complex $(Pb(N(CN)_2)_4)^{2-}$ and neutral complex $(M(N(CN)_2)_2L_2)$ (M = Pd, Pt), in which the amide nitro-

Corresponding authors: Jue Kou E-mail: koujue@ustb.edu.cn; Yi Xing E-mail: xingyi@ustb.edu.cn

gen atoms of $(N(CN)_2)^-$ are involved in the coordination reaction. Three modes of coordination between the dicyanamide anion and metal have been demonstrated in previous studies [1]: coordination by one of the terminal nitrogen atoms [9], double coordination via two terminal nitrogen atoms as in $Ag(N(CN)_2)$ [10], and quadruple coordination in $(CH_3)_2Ti(N(CN)_2)$.

In conclusion, the dicyanamide anion can react as a ligand, bridging metal ions to form a metal–dicyanamide coordination compound. Moreover, the dicyanamide anion behaves as a pseudochalcogeno-cyanate. Thus, we can hypothesize that the dicyanamide anion has some effects in gold leaching. To date, however, little attention has been given to its use in gold leaching.

In this study, leaching experiments were conducted to explore the leaching performance of the dicyanamide anion and to determine suitable leaching conditions. The quartz crystal microbalance with dissipation (QCM-D) technique was used to investigate the leaching kinetics of the dicyanamide anion, and the leaching products were analyzed using X-ray photoelectron spectroscopy (XPS) and electrospray mass spectrometry (ESI-MS) to identify Au complexes in the leach solution.

2. Materials and methods

2.1. Materials

To conduct the leaching experiments, we used gold concentrates obtained from a flotation process at the SQS Gold Mine, Fujian, China. Table 1 shows the chemical composition of the SQS gold concentrate. The test sample contained 62.68 g/t Au, 31.75% Fe, 30.52% S and 23.32% SiO_2. The element Au was in the form of natural gold. The contents of Cu, Pb, and Zn were determined to be very low. The XRD pattern of the ore sample is shown in Fig. 1. It can be seen that the mineral composition was simple. The main gold-bearing mineral was pyrite and the main gangue minerals were quartz and muscovite. Gold is not evident in the XRD pattern due to its low content.

Table 1. Chemical composition of the test sample wt%

Au*	Ag*	Fe	Cu	As	Zn
62.68	98.35	31.75	0.24	—	0.05
Pb	S	CaO	MgO	Al_2O_3	SiO_2
0.05	30.52	2.71	3.02	8.34	23.32

Note: * Unit is $g \cdot t^{-1}$.

2.2. Methods

2.2.1. Leaching test

For the leaching experiments, the SQS gold concentrate sample was ground to 90% –0.038 mm in a lab-scale ball mill. The leaching tests were conducted in a shaking water bath with 250 mL conical flasks. For each individual leaching test, 30 g of the ground sample was leached for 24 h at a constant solid/liquid mass ratio of 1:3 and a bath temperature of 30°C. The leaching solution was maintained at a pH value of 12 using sodium hydroxide, and the shaking frequency was set at 200 r/min. The leaching reagent solution was prepared by dissolving certain dosages of SD and potassium ferrocyanide (PF) simultaneously in distilled water. The leaching residuals from each test were then filtered and washed for gold assay. The pregnant leach solution was collected for XPS and ESI-MS analyses.

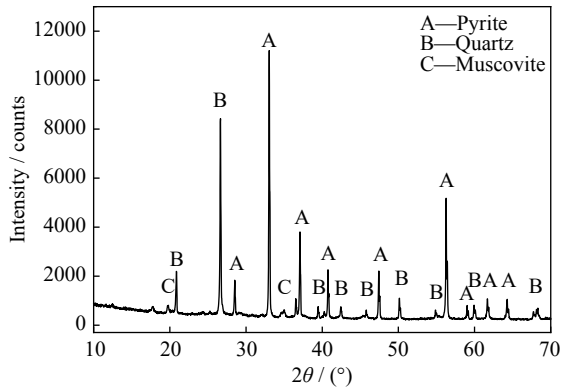

Fig. 1. XRD pattern of the test sample.

2.2.2. Quartz crystal microbalance with dissipation (QCM-D)

QCM-D is a type of device used for surface characterization analysis with high sensitivity. It is based on the quartz piezoelectric effect, which is used to monitor the surface reaction and quality changes synchronously in a liquid environment. When an alternating potential is applied, the quartz crystal exhibits mechanical oscillations. When the frequency of the alternating potential coincides with the frequency of the quartz crystal oscillation, recorded as f, piezoelectric resonance occurs. When the alternating potential is removed, its frequency decays exponentially and this attenuation is recorded as the energy dissipation factor D of the system [10–12]. Any mass changes (Δm) in the surface of the quartz crystal will trigger frequency changes (Δf), and these changes have a functional relationship. Thus the Δm value with time on the quartz crystal surface can be determined by recording the Δf, by which the dynamic of each reaction phase can be analyzed. By measuring changes in the energy dissipation (ΔD), the surface property changes of the quartz crystal can be identified.

Each QCM-D measurement was performed using a Q-Sense E4 system from Biolin Scientific, Sweden. The main working units comprise standard fluid modules that hold Q-Sensors, chamber platforms on which the modules are mounted, a peristaltic pump, and the electronics units [13]. All these units are connected to a computer. The control soft-

ware Q-Soft 401 is installed on the computer, which controls and records the various factors and signals, including the temperature, resonance, oscillation frequency, and energy dissipation factor. The core component of the QCM-D is the Q-sensor, which consists of an AT-cut quartz crystal sandwiched between two gold electrodes. The Q-sensor is 0.3-mm thick and 14 mm in diameter, and its fundamental resonance frequency is 5 MHz. The Q-Sensors used in this work were Au-coated quartz crystal sensors (QSX 301, gold surface) supplied by Q-Sense. The reaction surface area of the sensor was 0.2 cm^2 and it was coated with 100-nm-thick gold.

Prior to the leaching test, the sensors were cleaned with deionized water and dried with nitrogen. Then, the sensors were inserted into the standard fluid modules at a temperature of 30°C. When the Δf and ΔD signals had stabilized in the air, the buffer (distilled water with the same pH value as the reagents) was pumped into the system at a flow rate of 50 μL/min. After the Δf and ΔD had re-stabilized, a baseline was obtained, for which the variation was less than 1 Hz for at least 5 min. Once the baseline had been noted, the experiments were initiated. At a flow rate of 50 μL/min, the leaching solution was injected into the standard fluid modules to react with the gold on the surfaces of the sensors. After the increasing rate of the frequency curve had stabilized, the buffer was injected again at the same rate to rinse the surface. The purpose of this step was to determine whether the reaction was reversible. When the frequency curve reached a plateau, deionized water was pumped in to wash off the sensors for about 10 min, which ended the experiment. After the experiments had ended, analyses of the mass changes were performed using the Q-Sense Qtools 3.0 software based on the Sauerbrey and Voigt models. During this process, the Δf and ΔD values were determined at 0.5-s intervals.

When the ΔD value in an experiment is below 5×10^{-6}, the sensor's surface remains flat and uniform during the test and the mass changes in the surface can be interpreted as changes in the quartz crystal. Therefore, as described by the Sauerbrey equation [13–14], the change in mass (Δm) of the sensor's surface is directly proportional to $-\Delta f$:

$$\Delta m = -\frac{c\Delta f}{n} \quad (1)$$

where c = 17.8 $ng\cdot cm^{-2}\cdot Hz^{-1}$ is a mass sensitivity constant and n is the overtone number, whose value can be 1, 3, 5, 7, 9, or 11. In this study, the fifth overtone was used, which means the value of n was 5. When the change in the sensor's surface is viscoelastic, the Voigt model is used to analyze a change in mass [15]. Since the ΔD values obtained in this work were all below 5×10^{-6}, we applied the Sauerbrey equation for calculation and analysis.

2.2.3. X-ray photoelectron spectroscopy

XPS measurements were performed in ultrahigh vacuum conditions using an ESCALAB 250Xi instrument with an Al Kα source. The scanning area was 500 μm × 500 μm. The pass energy for the wide-energy spectrum was 70 eV, and narrow-energy scanning was performed using a pass energy of 20 eV and a step size of 0.05 eV. All the spectra were calibrated to the C 1s peak at 284.80 eV. Prior to the test, new sensors were characterized by XPS. After the test, the reagent-treated sensors were collected and rinsed with deionized water to remove residual reagents on the surface of the sensors. The sensors were then dried under vacuum and analyzed by XPS. The chemical compositions of the surfaces of the sensors were analyzed using a wide XPS energy spectrum, whereas the high-resolution spectra of the elements were obtained using narrow-energy scanning. The elemental composition of the sample was characterized by peak fitting using the Gaussian model XPS PEAK4.1 software.

2.2.4. Electrospray mass spectrometry

ESI-MS measurements were conducted in full scan detection mode in a Bruker microTOF-Q II instrument. The scan was initiated at mass-to-charge ratio m/z = 80 and ended at m/z = 1500. The nebulizer was used at a pressure of 0.08 MPa and dry gas at a speed of 4.0 L/min. The temperature of the dry heater was set at 180°C. The data was analyzed using Bruker data analysis software. During the QCM-D experiments, we collected the solution prior to leaching and the pregnant solution after leaching. The solution samples were then centrifuged and tested by ESI-MS.

3. Results and discussion

3.1. Leaching test

The effect of SD on gold recovery under different initial pH conditions was studied over a pH value range of 8 to 12 at an SD dosage of 30 kg/t. As shown in Fig. 2(a), when the initial pH of the system was below 9, the dissolution of gold in the SD solution was inefficient, with a gold recovery rate of less than 20%. When the initial pH was increased to above 9, gold recovery levels rose substantially and reached 32.8% at a pH value of 12. As such, gold recovery in the SD solution was found to be significantly influenced by the initial pH. Therefore, in high-alkalinity pulp, SD could dissolve gold relatively efficiently.

To investigate the effect of SD dosage on gold recovery, leaching tests were conducted at a constant pH value of 12 and different SD concentrations. As shown in Fig. 2(b), the gold recovery rate by self-leaching without any reagents was determined to be 9.7%. When the SD dosage was increased to 15 kg/t, the gold recovery rate increased rapidly to 34.8%, and then continued to fluctuate around 34% as the dosage was further increased. These results indicate that SD can dissolve gold in a high-alkalinity solution and that a saturation value is associated with the SD dosage, with higher dosages producing no further increase in the gold recovery rate.

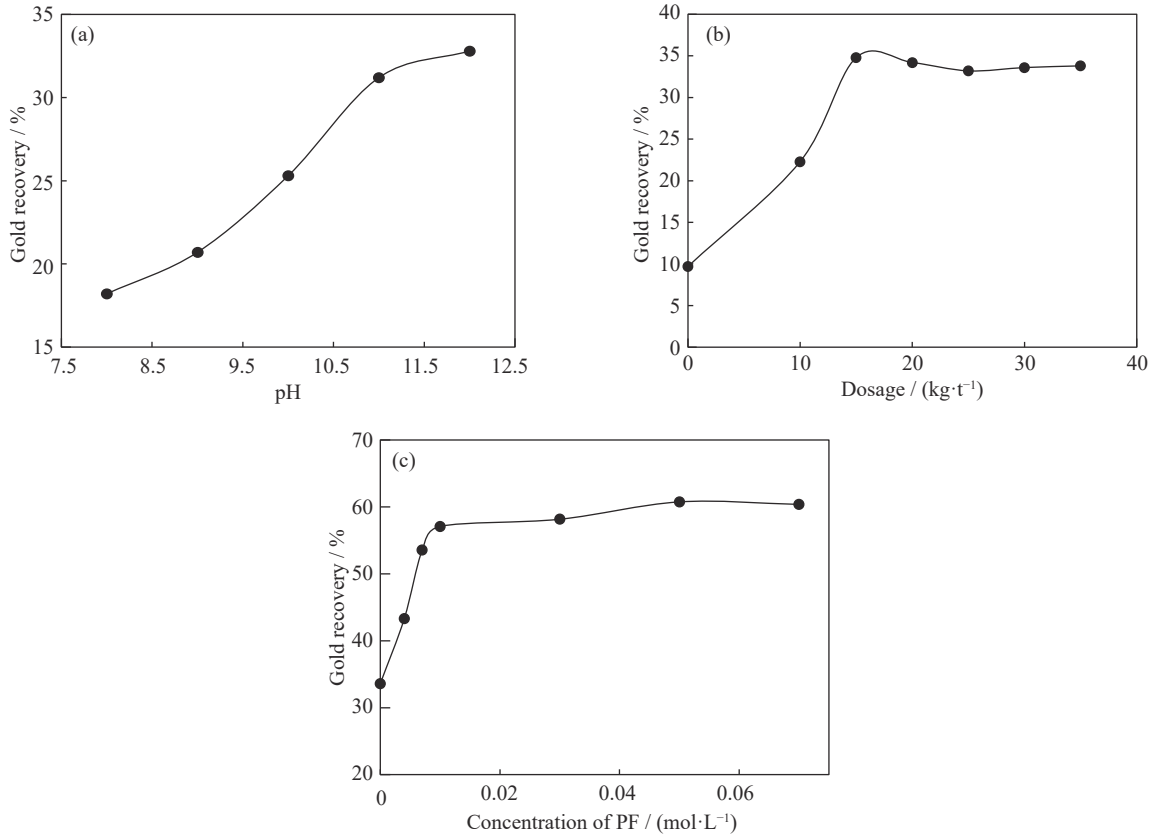

Fig. 2. Gold recovery rates as a function of initial pH (a), SD dosage (b), and PF concentration (c).

PF, whose chemical formula is $K_4Fe(CN)_6 \cdot 3H_2O$, is soluble in water. PF can ionize in water and form the anion $[Fe(CN)_6]^{4-}$, which has high mechanical and chemical stability [16]. The anion $[Fe(CN)_6]^{4-}$ also has strong binding ability with Cs^+, Sr^{2+}, Co^{2+}, Cu^{2+}, and some other metal ions.

Next, we investigated the effect of different PF concentrations on the gold recovery rate, again with a pH value of 12 and an SD dosage of 30 kg/t. As shown in Fig. 2(c), when the concentration of PF was increased from 0 to 0.01 mol/L, the gold recovery nearly doubled from 33.60% to 57.08%. When the concentration was further increased, the gold recovery rate fluctuated around 61%. These results indicate that the addition of PF can significantly improve the gold recovery in an SD solution.

3.2. QCM-D test

Using QCM-D, the gold-leaching process in a solution with different concentrations of SD and PF was monitored synchronously, and the leaching kinetics were analyzed. The data from the fifth overtone were used and the resonance frequency was 25 MHz.

3.2.1. Effect of different concentrations of sodium dicyanamide on leaching performance

Fig. 3 shows the frequency shift Δf and the dissipation shift ΔD of the leaching process in solutions with different SD concentrations as a function of time, with arrow 1 indicating the injection of the leaching reagent solution. In the figure, it is evident that the injection of the mixed solution of SD and PF caused a decrease in Δf and a sharp increase in ΔD, which indicates that the SD or PF might be adsorbed onto the surface of the sensor. With continuous injection of the mixed leaching solution, Δf reached its lowest point, and then began to rise at a constant rate. This suggests that the mixed solution of SD and PF had reacted with the Au on the surface of the sensor at a fixed rate. Meanwhile, the ΔD rose to an equilibrium state at values below 5×10^{-6}, indicating that the reaction between the leaching solution and Au had little effect on the surface viscoelasticity, which could be interpreted as rigid adsorption. When pumping the buffer into the system, Δf exhibited a slightly faster upward trend and ultimately reached equilibrium at non-zero values, whereas ΔD decreased nearly to its initial state, indicating that some irreversible reactions had occurred between the agent and Au and that the surface properties of the sensor had changed very little after this experiment.

As shown in Fig. 4, based on data of the frequency shift Δf and dissipation shift ΔD, the mass changes Δm of Au on the sensors' surface over time were obtained using the Sauerbray model, with all the ΔD values being below 5×10^{-6}. As shown in the graph, when the reagent was pumped into the system, as indicated by arrow 1, the Δm values initially increased, and then reached a peak, which might be the result

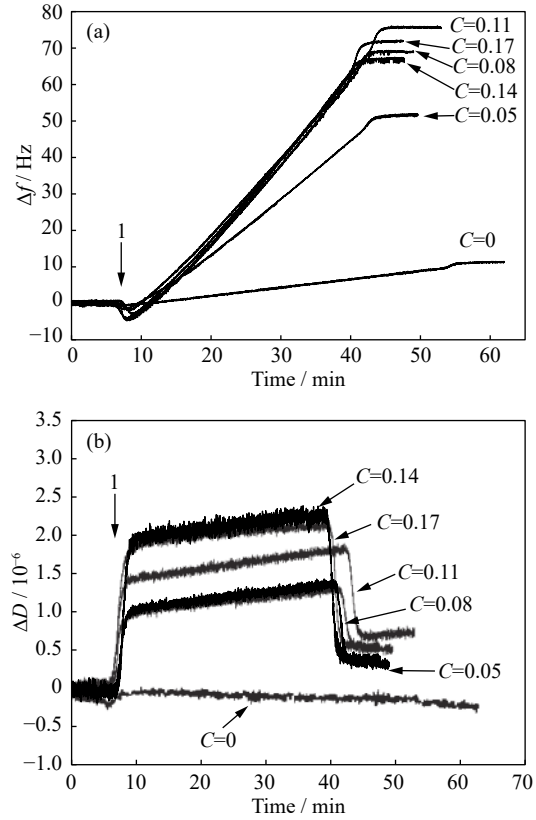

Fig. 3. Frequency shift Δf (a) and dissipation shift ΔD (b) versus leaching time at different SD concentrations C (mol/L) and 0.01 mol/L PF, pH = 12.

of the adsorption of the reagents onto the sensor's surface. With the successful injection of the reagent solution, the Δm values decreased and remained linear over time, which indicates that the agent solution had dissolved the gold on the sensor's surface. The SD concentration played an important role in the gold dissolution at low concentrations. When the concentration exceeded 0.08 mol/L, the gold-leaching rate stabilized.

3.2.2. Effect of different concentrations of potassium ferrocyanide on leaching performance

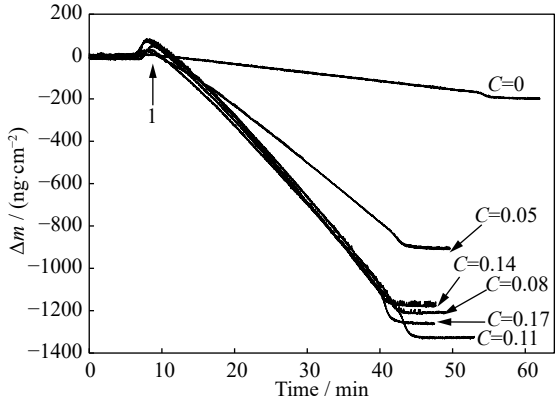

Fig. 4. Mass changes Δm versus leaching time at different SD concentrations C (mol/L) and 0.01 mol/L PF, pH = 12.

Fig. 5 shows the frequency shift Δf and dissipation shift ΔD of the leaching process in the agent solution at different PF concentrations and an SD concentration of 0.11 mol/L as a function of time. As shown in the graph, Δf and ΔD follow similar change rules as those observed in the SD concentration experiments. During these tests, Δf reached an equilibrium at non-zero values, and the ΔD values were all below 5×10^{-6}. As shown in Fig. 6, the mass changes Δm of Au on the sensors' surface over time were calculated according to the Sauerbray model.

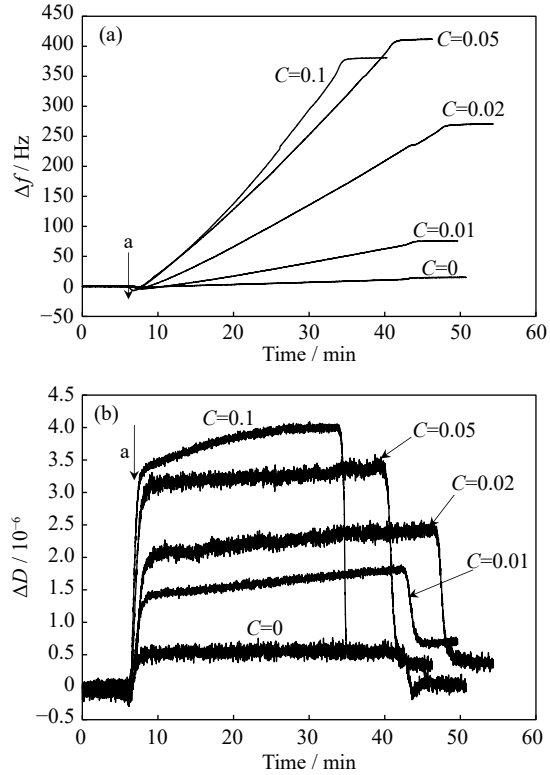

Fig. 5. Frequency shift Δf (a) and dissipation shift ΔD (b) versus leaching time at different PF concentrations. The SD concentration was 0.11 mol/L and the pH was 12.

In Fig. 6, we can see that once the leaching solution of SD with PF was injected into the system, the mass change of the sensor (Δm) increased immediately. With continuous injection of the solution, Δm increased at a constant rate. The mass change rate of the sensor increased with increases in the PF concentration, which suggests that PF has a positive effect on the gold-leaching rate of an SD solution.

3.2.3. Leaching kinetics analysis

The rate of mass change, i.e., the leaching rate of gold, was calculated based on the Δm–time graph. Fig. 7(a) shows the relationship between the leaching rate and the SD concentration. When no SD was added, the leaching rate was 4.03 ng·cm^{-2}·min^{-1}, which suggests that PF alone cannot efficiently dissolve gold. When the SD concentration was in-

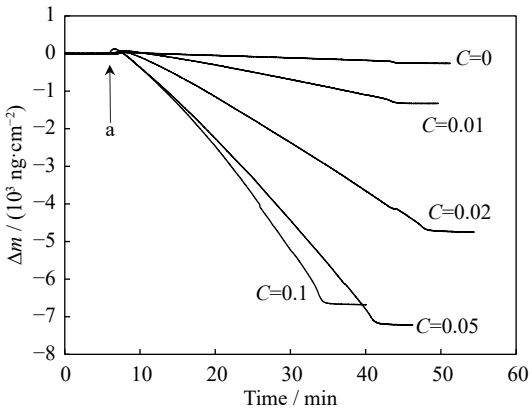

Fig. 6. Mass changes Δ*m* versus leaching time at different PF concentrations. The SD concentration was 0.11 mol/L and the pH was 12.

creased from 0 to 0.08 mol/L, the leaching rate increased linearly and reached 36.97 ng·cm^{-2}·min^{-1} at 0.08 mol/L, which implies that the leaching reaction is SD-diffusion-controlled. At an SD concentration >0.08 mol/L, the leaching rate reached its steady-state value. Therefore, to achieve a rapid leaching rate, an SD concentration >0.08 mol/L must be maintained.

Fig. 7(b) shows the relationship between the leaching rate and the PF concentration, in which the leaching rate increased from 38.38 to 272.62 ng·cm^{-2}·min^{-1} with increases in the PF concentration from 0.01 mol/L to 0.1 mol/L. This indicates that PF significantly improved the gold-leaching rate. As shown in Fig. 7, the data are not linear, and initially the leaching rate increases much faster. This result implies that the reaction is not PF-diffusion–controlled, but, most probably, chemically controlled.

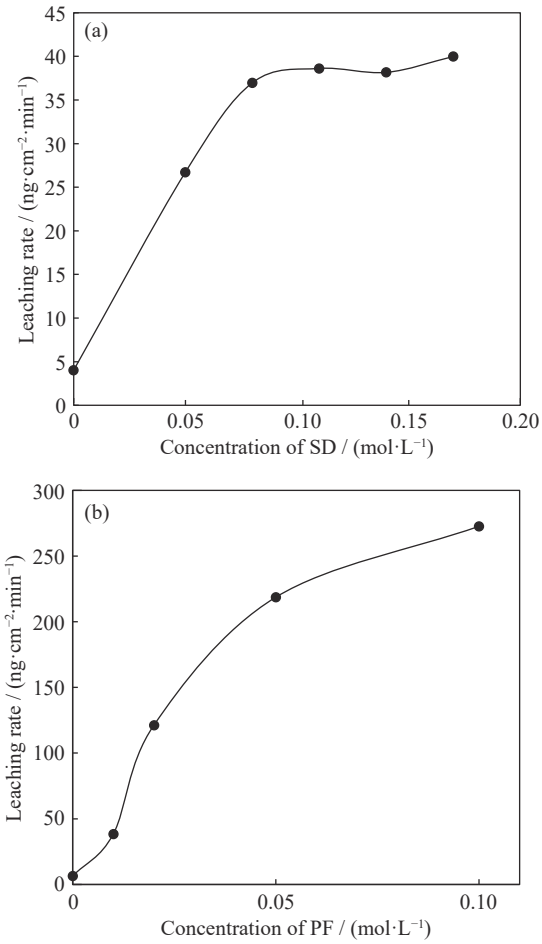

Fig. 7. Leaching rate versus SD concentration (a) and PF concentration (b).

3.3. XPS analysis of the leached sensor surface

Next, quartz crystal sensors were analyzed by XPS before and after leaching in a solution of 0.11 mol/L SD and 0.02 mol/L PF. The XPS wide-energy spectrum of the clean and agent-treated sensor was obtained to determine the chemical composition of the Au surface. As can be seen in Fig. 8, the surface of the clean sensor mainly contained the element Au 4f with small amounts of elements C 1s and O 1s. This confirms that gold had been successfully coated onto the surface of the sensor without the addition of any impurities. After leaching, the relative contents of elements C 1s and O 1s increased substantially, and a new element N 1s appeared, which indicates that the elements C 1s, O 1s, and N 1s had been deposited onto the sensor surface after the leaching process, which resulted in the formation of some complexes.

To further study the species and bonding characteristics of

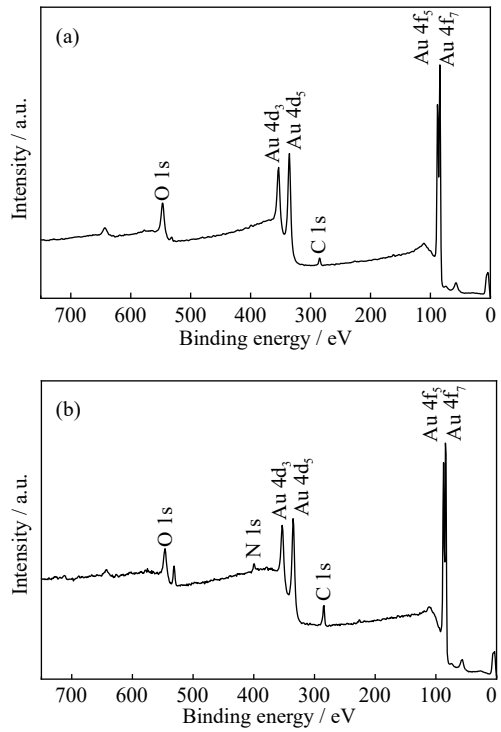

Fig. 8. XPS wide-energy spectrum of the clean and leached sensors: (a) before leaching; (b) after leaching.

the elements, we obtained the high-resolution spectra of the elements through narrow-energy scanning. XPS PEAK4.1 software was used for peaking fitting.

3.3.1. XPS analysis of element Au 4f

Fig. 9 shows the high-resolution XPS spectra of Au 4f on the surface of the clean and reagent-treated sensor before and after leaching. It is interesting that the Au content on the surface of the reagent-treated sensor is significantly lower than that on the surface of the clean sensor, which indicates that most of the Au had dissolved into the reagent solution. According to the Handbook of X-ray Photoelectron Spectroscopy and related studies, Au $4f_{7/2}$, Au^{+} $4f_{7/2}$, and Au^{3+} $4f_{7/2}$ peaks appear at 83.8, 85, and 86 eV, respectively. As revealed in the XPS analysis, the existence of Au on the clean sensor surface is evidenced by the main peak at 83.98 eV. After leaching, the main peak shifted to 84.43 eV, the binding energy of which is between that of the clean sensor (83.98 eV) and Au^{+} (approximately 85 eV). On one hand, the main peak (84.43 eV) of the reagent-treated sensor exhibits an obvious offset toward higher binding energies compared to that (83.98 eV) of the clean sensor. This shift results from changes in the charge distribution of the Au atoms, whereby the density of the outer electrons decreases and the bonding energy of the inner electrons increases, resulting in a chemical shift toward a higher binding energy. This indicates the formation of some that are positively charged Au. On the other hand, the binding energy of the Au $4f_{7/2}$ (83.98 eV) of the reagent-treated sensor is much lower than that (approximately 85 eV) of Au^{+} $4f_{7/2}$. This suggests that Au has bonded with other ions or groups to form complex ions after oxidation to Au^{+}. According to the principles of charge transfer [17], during the formation of a complex ion, the charges belonging to an atom change and cause a chemical shift in the XPS spectrum. After oxidation to Au^{+}, the Au atom undergoes a coordination reaction, in which it accepts charges from other atoms, which leads to a decrease in its binding energy.

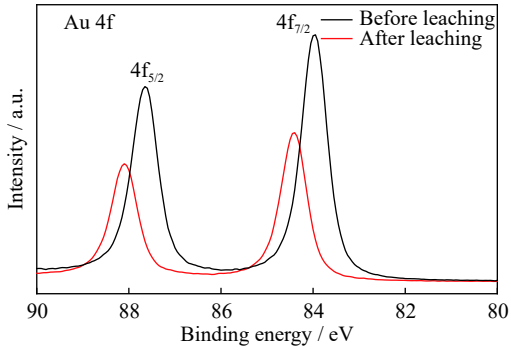

Fig. 9. XPS spectra of Au 4f before and after leaching.

3.3.2. XPS analysis of element C 1s

Fig. 10 shows the high-resolution XPS spectra of element C 1s on the surface of both the clean and reagent-treated sensors. As can be seen, the relative content of the element C 1s has increased with the main peak of C 1s appearing at 284.8 eV, owing to traces of pre-adsorbed hydrocarbon contamination on the sensor surface [18–19]. The spectra exhibit significant asymmetric characteristics and a chemical shift of the C 1s peak after leaching, which indicate the existence of other carbon-containing species of C 1s. Consequently, we performed peak fitting to analyze the forms of C 1s.

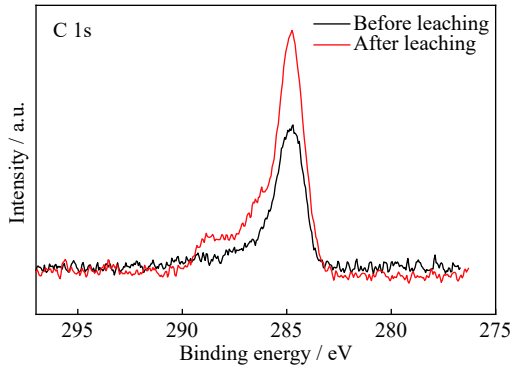

Fig. 10. XPS spectra of C 1s before and after leaching.

Fig. 11 shows the XPS spectra of element C 1s after peak fitting. Before leaching, three peaks at 284.84, 286.70 and 289.24 eV were noted in the XPS spectrum. The peaks at 284.84 and 286.70 eV correspond to traces of organic pollutants pre-adsorbed onto the sensor's surface, and the peak with lower intensity at 289.24 eV is assigned to either the C═O or O═C—H of the carbonate produced by carbon di-

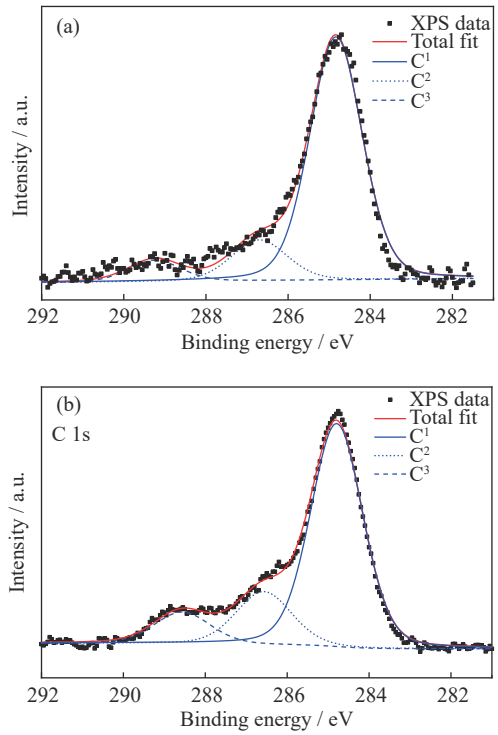

Fig. 11. C 1s peaks of sensors before and after leaching: (a) before leaching; (b) after leaching.

oxide adsorbed onto the sensor's surface [18–20]. After treatment with the leaching reagent, the XPS spectrum of element C 1s makes three contributions, C^1, C^2 and C^3, located respectively at 284.76, 286.42, and 288.56 eV. C^1 corresponds to carbon–hydrogen bonds (C—H) or carbon–carbon bonds (C—C), and C^2 indicates the existence of carbon–nitrogen bonds (C—N) that correspond to complexes formed during the leaching process. The C^3 peak at 288.56 eV is characteristic of the cyano group (C≡N) in the complexes formed during the leaching process [21].

3.3.3. XPS analysis of element N 1s

No obvious characteristic peaks of N 1s could be detected from the spectrum of the surface of the clean sensor. Fig. 12 shows the high-resolution XPS spectrum of element N 1s of the agent-treated sensor, which clearly indicates the presence of three chemical environments of nitrogen atoms. The N^1 peak at 399.86 eV corresponds to the cyano group (C≡N) and the N^3 peak at 399.86 eV is assigned to carbon–nitrogen bonds (C—N), which is in agreement with the analysis of C 1s. In accordance with the analysis of Au 4f, the high binding energy N^2 peaks at 401.3 eV thus characterize nitrogen atoms that are bonded with Au atoms in complexes formed during the leaching process.

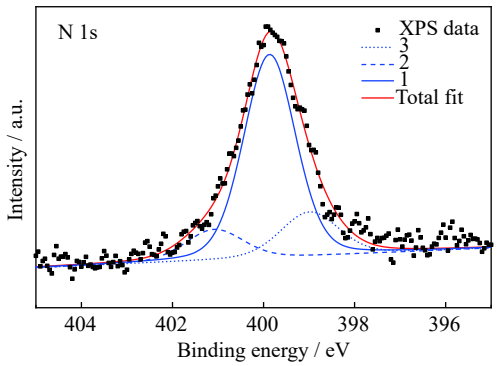

Fig. 12. XPS spectrum of element N 1s after leaching.

3.3.4. XPS analysis of element O 1s

Fig. 13 shows the high-resolution XPS spectrum of element O 1s on the surfaces of the clean and reagent-treated sensors, in which the relative content of O 1s exhibits a sharp rise. The main peak of O 1s occurs at approximately 531.8 eV, representing hydroxyl (OH^-). To further explore the existing oxygen-containing species, a peak fitting of O 1s was conducted, as shown in Fig. 14.

In Fig. 14, there are three peaks at 531.83, 530.68, and 533.06 eV. The greatest intensity at O^1 (531.83 eV) is attributed to hydroxyl (OH^-), indicating the presence of aurum hydroxide. The peak at O^2 (530.68 eV) is attributed to O^{2-}, which indicates the appearance of a metal oxide. The high binding energy O^3 at 533.06 eV is assigned to H_2O as the test was conducted in aqueous solution and the surface has the characteristics of water even though it had been dried prior to XPS analysis [22].

The results of the XPS analysis demonstrate that the Au and $(N(CN)_2)^-$ formed complex ions consisting of C≡N, C—N, and N—Au. Based on this information, it can be presumed that complexes such as $(Au(N(CN)_2)_2)^-$or $AuN(CN)_2$ were formed during the leaching process. Moreover, the XPS spectrum of element O 1s indicates the presence of aurum hydroxide and aurum oxide during the leaching process.

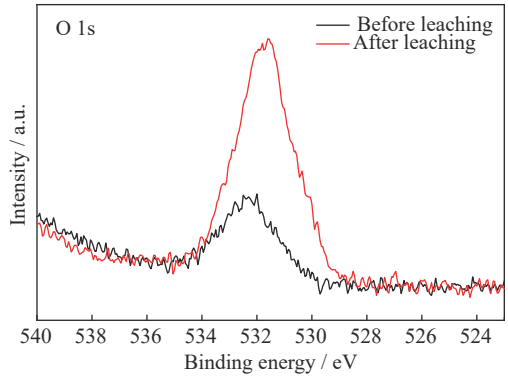

Fig. 13. XPS spectrum of element O 1s before and after leaching.

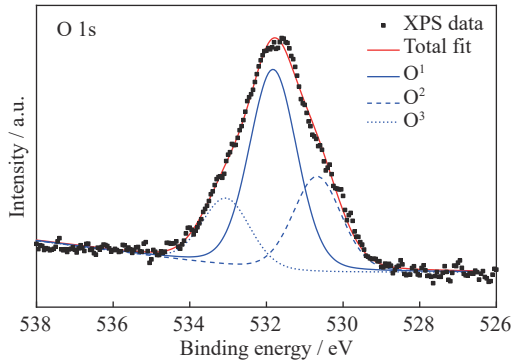

Fig. 14. XPS spectrum of element O 1s after leaching.

3.4. ESI-MS analysis of pregnant solution

To further investigate the composition of the leaching products, a QCM-D test was conducted in a 0.11 mol/L SD solution and the pregnant solution was collected and analyzed by ESI-MS. Fig. 15 shows the ESI-MS spectra of the SD solution before and after leaching. In these spectra, the *m*/*z* value of each peak was considered to be the relative molecular mass of each solute. As shown in Fig. 15, the dissolved ions in the pregnant solution were almost the same as those in the original SD solution, except they ranged from *m*/*z* = 300 to *m*/*z* = 700. In this range, several peaks with non-negligible intensities appeared, and the analysis of these peaks is shown in Fig. 16.

As shown in Fig. 16, several new peaks appeared after leaching at *m*/*z* values of 328.9786, 417.9679, 506.9759, 595.9713, and 684.9801, and the difference between any two

adjacent new peaks was about 89, which is the relative molecular mass of $NaN(CN)_2$. These products were analyzed based on the XPS results and their relative molecular masses, the results of which are shown in Table. 2.

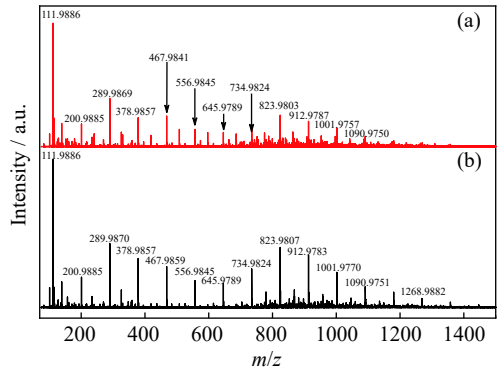

Fig. 15. ESI-MS spectra of the SD solutions: (a) pregnant solution; (b) original SD solution.

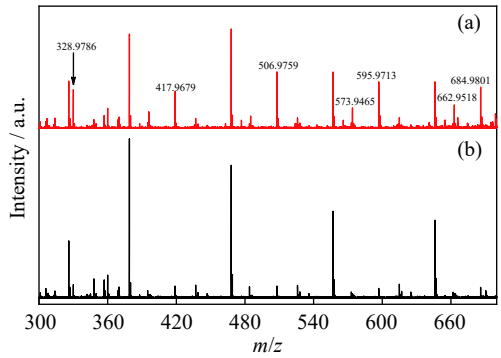

Fig. 16. ESI-MS spectrum of the solutions before and after leaching (m/z = 300–700): (a) pregnant solution; (b) original SD solution.

Table 2. Products formed during leaching

m/z	Formula
328.9786	$[Au(N(CN)_2)_2]^-$
417.9679	$[AuNa(N(CN)_2)_3]^-$
506.9759	$[AuNa_2(N(CN)_2)_4]^-$
595.9713	$[AuNa_3(N(CN)_2)_5]^-$
684.9801	$[AuNa_4(N(CN)_2)_6]^-$

As shown in Table 2, the anionic coordination groups $[Au(N(CN)_2)_2]^-$, $[AuNa(N(CN)_2)_3]^-$, $[AuNa_2(N(CN)_2)_4]^-$, $[AuNa_3(N(CN)_2)_5]^-$, and $[AuNa_4(N(CN)_2)_6]^-$ were found in the pregnant solution from the SD leaching test. Therefore, $[N(CN)_2]^-$ can directly react with Au to form $[Au(N(CN)_2)_2]^-$. Moreover, $[AuNa(N(CN)_2)_3]^-$ and other groups can be formed in two ways: (a) a continuous reaction of $[Au(N(CN)_2)_2]^-$ with $NaN(CN)_2$ leading to the formation of metal complex ions, $[AuNa_x(N(CN)_2)_{x+2}]^-$ (x = 1, 2, 3, or 4); (b) a direct reaction of $[Na_x(N(CN)_2)_{x+2}]^{2-}$ ions present in the SD solution with Au to form coordination groups.

4. Conclusions

Based on the results of sodium dicyanamide leaching tests, and the analysis of the leaching residuals, the following conclusions can be drawn:

(1) Sodium dicyanamide (SD) is able to dissolve gold in a high-alkalinity solution. However, the gold recovery was only 34.8% when SD was used as the sole leaching reagent at an optimal dosage. The addition of potassium ferrocyanide (PF) was found to significantly improve gold recovery. In the presence of 0.01 mol/L PF in the SD solution, the gold recovery rate increased from 34.8% to 57.08%.

(2) Dicyanamide ions underwent a coordination reaction with Au and formed a series of complex ions, $[AuNa_x(N(CN)_2)_{x+2}]^-$ (x = 1, 2, 3, or 4). $[N(CN)_2]^-$ directly reacted with Au to form $[Au(N(CN)_2)_2]^-$. However, $[AuNa(N(CN)_2)_3]^-$ and other ions formed in two ways: (a) a continuous reaction of $[Au(N(CN)_2)_2]^-$ with $NaN(CN)_2$ leading to the formation of the series $[AuNa_x(N(CN)_2)_{x+2}]^-$ (x = 1, 2, 3, or 4), and (b) a reaction of $[Na_x(N(CN)_2)_{x+2}]^{2-}$ with Au to form coordination groups.

Acknowledgement

The authors would like to thank the National Naturel Science Foundation of China (Nos.51974016 and 51204012) for financial support.

References

[1] C.B. Sun, X.L. Zhang, J. Kou, and Y. Xing, A review of gold extraction using noncyanide lixiviants: Fundamentals, advancements, and challenges toward alkaline sulfur-containing leaching agents, *Int. J. Miner. Metall. Mater.*, 27(2020), No. 4, p. 417.

[2] H. Qin, X.Y. Guo, Q.H. Tian, and L. Zhang, Recovery gold from refractory gold ore: Effect of pyrite on the stability of the thiourea leaching system, *Int. J. Miner. Metall. Mater.*, https://doi.org/10.1007/s12613-020–2142-9.

[3] H.F. Zhao, H.Y. Yang, L.L. Tong, Q. Zhang, and Y. Kong, Biooxidation-thiosulfate leaching of refractory gold concentrate, *Int. J. Miner. Metall. Mater.*, 27(2020), No. 8, p. 1075.

[4] D. Britton, Silver dicyanamide, $AgN(CN)_2$-orthorhombic modification, *Acta Crystallogr., Sect. C*, 46(1990), No. 12, p. 2297.

[5] P.M. Van Der Werff, S.R. Batten, P. Jensen, B. Moubaraki, and K.S. Murray, Cation templation of anionic metal dicyanamide networks, *Inorg. Chem.*, 40(2001), No. 7, p. 1718.

[6] M. Kurmoo and C.J. Kepert, Hard magnets based on transition metal complexes with the dicyanamide anion, $\{N(CN)_2\}^-$, *New J. Chem.*, 22(1998), No. 12, p. 1515.

[7] L.Y. Zhang, L.X. Shi, and Z.N. Chen, Syntheses, structures, and electronic interactions of dicyanamide/tricyanomethanide-bridged binuclear organometallic complexes, *Inorg. Chem.*, 42(2003), No. 2, p. 633.

[8] J. Kohout, L.Jäger, M. Hvastijová, and J. Kožíšek, Tricyanomethanide and dicyanamide complexes of Cu(II), Ni(II), Co(II), their structures and properties, *J. Coord. Chem.*, 51(2000), No. 2, p. 169.
[9] S.R. Batten and K.S. Murray, Structure and magnetism of coordination polymers containing dicyanamide and tricyanomethanide, *Coord. Chem. Rev.*, 246(2003), No. 1–2, p. 103.
[10] D. Britton and Y.M. Chow, The crystal structure of silver dicyanamide, $AgN(CN)_2$, *Acta Crystallogr., Sect. B*, 33(1977), No. 3, p. 697.
[11] M.I. Jeffrey, J. Zheng, and I.M. Ritchie, The development of a rotating electrochemical quartz crystal microbalance for the study of leaching and deposition of metals, *Meas. Sci. Technol.*, 11(2000), No. 5, p. 560.
[12] I.C. Chen and M. Akbulut, Nanoscale dynamics of heavy oil recovery using surfactant floods, *Energy Fuels*, 26(2012), No. 12, p. 7176.
[13] J. Kou and S.H. Xu, In situ kinetics and conformation studies of dodecylamine adsorption onto zinc sulfide using a quartz crystal microbalance with dissipation (QCM-D), *Colloids Surf. A*, 490(2016), p. 110.
[14] C. Gutig, B.P. Grady, and A. Striolo, Experimental studies on the adsorption of two surfactants on solid−aqueous interfaces: adsorption isotherms and kinetics, *Langmuir*, 24(2008), No. 23, art. No. 13814.
[15] P. Josefsson, G. Henriksson, and L. Wågberg, The physical action of cellulases revealed by a quartz crystal microbalance study using ultrathin cellulose films and pure cellulases, *Biomacromolecules*, 9(2008), No. 1, p. 249.
[16] M. Rodahl and M. Jonson, Viscoelastic acoustic response of layered polymer films at fluid-solid interfaces: Continuum mechanics approach, *Phys. Scripta*, 59(1999), No. 5, p. 391.
[17] Y.X. Da, Y.Q. Liu, and X.C. Zhu, XPS study on polytetramethylene porphyrin and its metal complexes, *Acta Chim. Sinica*, 43(1985), No. 1, p. 44.
[18] S.H. Xu, J. Kou, T.C. Sun, and K. Jong, A study of adsorption mechanism of dodecylamine on sphalerite, *Colloids Surf. A*, 486(2015), p. 145.
[19] Z.S. Hua, G.C. Yao, J. Ma, Z.G. Zhang, and L.S. Liang, XPS analysis of nickel layers on carbon fiber, *Chin. J. Nonferrous Met.*, 21(2011), No. 1, p. 165.
[20] D. Kowalczyk, S. Slomkowski, M.M. Mohamed, and M. Delamar, Adsorption of aminopropyltriethoxy silane on quartz: an XPS and contact angle measurements study, *Int. J. Adhes. Adhes.*, 16(1996), No. 4, p. 227.
[21] Z.C. Wang, Y.Z. Zhang, S.M. Zhou, and C.J. Lin, Corrosion compositions of carbon steel under ion-selective coatings by XPS, *J. Chin. Soc. Corros. Prot.*, 21(2001), No. 5, p. 273.
[22] R. Pietrzak, T. Grzybek, and H. Wachowska, XPS study of pyrite-free coals subjected to different oxidizing agents, *Fuel*, 86(2007), No. 16, p. 2616.